arXiv:1704.00199v1 [physics.ins-det] 1 Apr 2017

Improved Electromagnetic Phase-Shift Flowmeter for Liquid Metals with Variable Conductivity

Richard Looney and Jānis Priede

Applied Mathematics Research Centre, Coventry University, UK

Abstract. We present a concept of improved phase-shift flowmeter that has a significantly reduced sensitivity to the variation of the electrical conductivity of liquid metal. A simple theoretical model of flowmeter is considered where the flow is approximated by a solid finite-thickness conducting layer moving in the presence of ac magnetic field. In contrast to the original design [Priede et al., Meas. Sci. Technol. 22 (2011) 055402], where the flow rate is determined by measuring only the internal phase shift between the voltages induced in two receiving coils, the improved design measures also the external phase shift between the sending and the upstream receiving coil. We show that the effect of electrical conductivity can be strongly reduced on the flow-induced internal phase shift, when it is properly rescaled with the external phase shift, which depends mostly on the conductivity of medium. Two different rescalings are found depending on the ac frequency. At low frequencies when the shielding effect is negligible, the effect of conductivity is strongly reduced by rescaling the internal phase shift with the external one squared. At higher frequencies, the same is achieved by rescaling the internal phase shift directly with the external one.

Keywords: Electromagnetic flowmeter, liquid metal, ac magnetic field

PACS numbers: 41.20.Gz, 47.60.Dx, 47.65.-d, 47.80.Cb

Submitted to: *Meas. Sci. Technol.*

1. Introduction

Electromagnetic flow metering based on the voltage induced between the electrodes in contact with a conductive liquid that flows in the presence of magnetic field dates back to Faraday [4]. Now it is a well established flow metering technique which works reliably for common liquids with conductivities as low as that of tap water, i.e., a few μS/cm [1]. Application of this standard technique to liquid metals is however hampered by various of contact problems ranging from the corrosion of electrodes to spurious electrochemical and thermoelectric potentials [15]. The effect of spurious potentials can be mitigated by using pulsed magnetic field [22] which has been suggested earlier as a possible solution against the electrode polarisation in a biomedical fluid [18]. The corrosion problem could in principle be avoided by using capacitately-coupled electrodes to measure the induced voltage in contactless way [7, 9].

There are several other more widely used contactless flow metering methods for liquid metals which rely on the eddy currents induced by the flow in the magnetic field. As first suggested by Shercliff [17] and later pursued by the so-called Lorentz Force Velocimetry [21], the flow rate can be determined by measuring the force generated by eddy currents on a magnet placed close to the flow of conducting liquid. Alternative approach, which is virtually force-free and thus largely independent of the conductivity of liquid metal [12], is to determine the flow rate from the equilibrium rotation rate of a freely rotating magnetic flywheel [16, 2] or just a single magnet [14]. More common are the contactless eddy-current flow meters which measure the the flow-induced perturbation of externally applied magnetic field [8, 3, 11]. This principle underlies also the so-called flow tomography approach, where the spatial distribution of the induced magnetic field is analysed [20, 19].

The main challenge of the eddy current flowmeters is the weak induced magnetic field with a relative amplitude of the order of magnitude of the magnetic Reynolds number $Rm \sim 10^{-4} - 10^{-1}$ which has to be measured in the presence of a much stronger external magnetic field. Although the background signal produced by the transformer effect of the applied magnetic field can be compensated by a proper arrangement of sending and receiving coils [5] this type of flow meter remains highly susceptible to small geometrical imperfections and disturbances. Recently, it was shown that the sensitivity of the eddy current flowmeter to such geometrical disturbances can be greatly reduced when instead of the usual amplitude difference one measures the phase shift induced by the flow between two receiver coils [13]. This is because the phase is determined by the ratio of two amplitudes and, thus, it remains invariant when both amplitudes are perturbed in the same way so that they remain nearly proportional to each other. The phase shift induced by the flow was found to depend not only on the velocity but also on the conductivity of liquid metal. The susceptibility to varying conductivity, which is a general problem affecting not only eddy-current but also the Lorentz force devices, is the main drawback of the phase-shift flowmeter. While there are devices which can address this problem such as the single magnet rotary flowmeter [14] or the transient

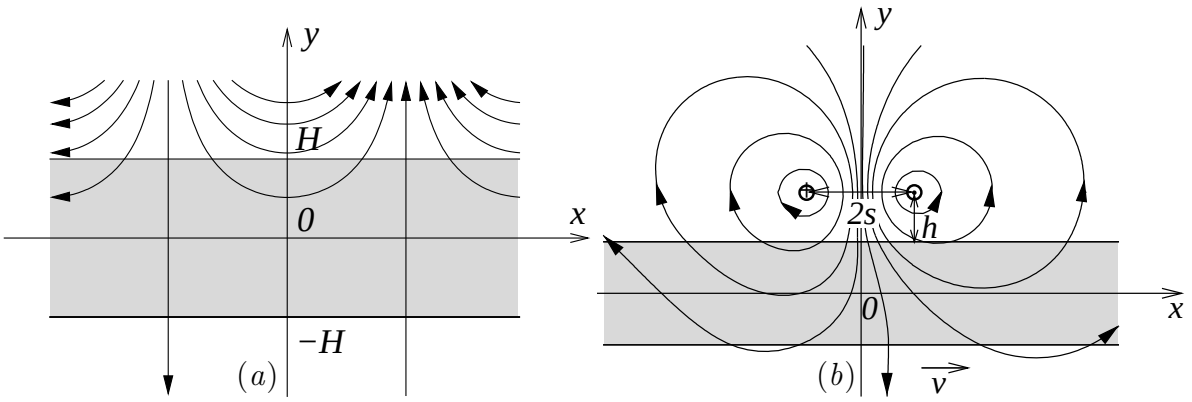

Figure 1. Model of a conducting layer of thickness $2H$ in an external magnetic field represented by a standing harmonic wave (a) and generated by a couple of straight wires (b).

eddy-current flowmeter [6], they come with other drawback such as moving parts for the former and a relative complicated measurement scheme for the latter.

This paper is concerned with the development of the recently invented ac induction flowmeter for liquid metal flows based on the phase shift measurements. We present a refined measurement scheme with a reduced dependence on conductivity. The idea is that not only the eddy currents induced by the liquid flow but also those induced by the alternating magnetic field itself give rise to the phase shift in the induced magnetic field. The latter effect, which leads to the phase shift between the sending and receiving coils, is dependant on the conductivity of the liquid. Therefore it may be used to compensate for the effect of conductivity on the flow-induced phase shift. The feasibility of such an approach will be investigated using two simple theoretical models of the phase-shift flowmeter, where the flow is approximated by a solid body motion of a finite-thickness conducting layer.

The paper is organised as follows. Mathematical model and the basic equations describing the phase-shift flowmeter are briefly recalled in the next section. In Section 3 we present and discus numerical results for two simple configurations of the applied magnetic field: the first in the form of a mono-harmonic standing wave and the second generated by a simple coil made of couple of straight wires placed above the layer. The paper is concluded by a summary in Section 4. Relevant mathematical details of solutions behind numerical results are provided in the Appendix.

2. Mathematical Model

Following Priede et al. [13] we consider an alternating magnetic field with induction $\boldsymbol{B}$ in the presence of a conductive medium of thickness $2H$ and infinite horizontal extension shown in figure 1. The medium travels at a velocity of $\boldsymbol{v} = \boldsymbol{e}_x v$ and has conductivity σ. The induced electric field is governed by the Maxwell-Faraday equation as $\boldsymbol{E} = -\boldsymbol{\nabla}\Phi - \partial_t \boldsymbol{A}$, where Φ is the electric potential and $\boldsymbol{A}$ is the vector potential,

which defines the magnetic field as $\boldsymbol{B} = \boldsymbol{\nabla} \times \boldsymbol{A}$. The density of the electric current induced in the moving medium is given by Ohm's law

$$\boldsymbol{j} = \sigma(\boldsymbol{E} + \boldsymbol{v} \times \boldsymbol{B}) = \sigma(-\boldsymbol{\nabla}\Phi - \partial_t \boldsymbol{A} + \boldsymbol{v} \times \boldsymbol{\nabla} \times \boldsymbol{A}),$$

where Φ is the electric potential. Subsequently, we consider a 2D magnetic field which is invariant along the unit vector $\boldsymbol{e}_z$ and alternates in time harmonically with the angular frequency ω. Firstly, such a magnetic field can be described by the vector potential with a single component $\boldsymbol{A} = \boldsymbol{e}_z A$ as $\boldsymbol{B} = -\boldsymbol{e}_z \times \boldsymbol{\nabla} A$, where $\boldsymbol{B}$ has only two components in the (x, y) plane. Note that $\boldsymbol{B} \cdot \boldsymbol{\nabla} A \equiv 0$, which means that the isolines of A represent the flux lines of $\boldsymbol{B}$. Secondly, it can be sought in the complex form $A(\boldsymbol{r}, t) = \Re\left[A(\boldsymbol{r}) e^{ß\omega t}\right]$, where $A(\boldsymbol{r})$ is the complex amplitude distribution and $\boldsymbol{r}$ is the radius vector.

Assuming that the frequency is sufficiently low and, thus, the displacement current is negligible, Ampere's law $\boldsymbol{j} = \mu_0^{-1} \boldsymbol{\nabla} \times \boldsymbol{B}$ leads to $\Phi \equiv 0$ and the following advection-diffusion equation for $A(\boldsymbol{r})$

$$\mu_0 \sigma(ß\omega A + v \partial_x A) = \boldsymbol{\nabla}^2 A, \tag{1}$$

where $\mu_0 = 4\pi \times 10^{-7}\,\mathrm{H/m}$ is the vacuum permeability. The continuity of $\boldsymbol{B}$ at the interface S between the conducting medium and free space requires

$$[A]_S = [(\boldsymbol{n} \cdot \boldsymbol{\nabla})A]_S = 0, \tag{2}$$

where $[]_S$ denotes a jump across S and $\boldsymbol{n}$ the unit normal to S.

We consider the same two configurations of the applied magnetic field studied by Priede et al. [13]. The first is a mono-harmonic standing wave with the wave number k in the x-direction

$$A_0(\boldsymbol{r}, t) = \hat{A}_0(y) \cos(kx) \cos(\omega t), \tag{3}$$

which is shown in figure 1(a). The second is a magnetic field generated by the finite-size coil which consists of two parallel straight wires fed with an ac current of amplitude I_0 flowing in the opposite directions along the z-axis at distance $2s$ in the x-direction and placed at height h above the upper surface of the layer as shown in figure 1(b). The analytical and semi-analytical solutions, which underlay the following numerical analysis, can be found in Ref. [13]. To make the paper self-contained a brief summary of solution is provided in the Appendix.

The two key parameters which appear in the problem are the dimensionless ac frequency $\bar{\omega} = \mu_0 \sigma \omega H^2$ and the magnetic Reynolds number $Rm = \mu_0 \sigma v H$. The latter defines velocity of the layer in the units of the characteristic magnetic diffusion speed $(\mu_0 \sigma H)^{-1}$ and is subsequently referred to as the dimensionless velocity. We shall use also the ratio $Rm/\bar{\omega} = v/(\omega H)$, which defines the velocity of layer relative to the characteristic phase speed of the magnetic field and is referred to as the relative velocity.

For the physical interpretation of the results let us recall that the circulation of vector potential along a closed contour gives a magnetic flux through the encircled surface. For the simple 2D case under consideration, when the vector potential has only one component, the difference of the vector potential between two points defines the

linear flux density between two lines parallel to the vector potential at those two points. The same holds also for the time derivative of the corresponding quantities. Thus, the difference of the vector potential amplitudes between two points is proportional to the voltage amplitude which could be measured by an idealised coil consisting of two straight parallel wires placed along the z-axis at those points. Correspondingly, the single-point vector potential gives the voltage measured by a 'wide' coil with the second wire placed sufficiently far away in the region of a negligible magnetic field.

3. Numerical Results

3.1. Mono-Harmonic Magnetic Field

Let us start with a simple external magnetic field in the form a mono-harmonic standing wave (3) and first briefly recall the basic characteristics of the original phase-shift flowmeter [13]. When the layer is at rest ($Rm = 0$), the induced magnetic field forms a standing wave like the external field. Because the adjacent halves of a standing wave oscillate in the opposite phases, the phase distribution is discontinuous along the wave and jumps by π across its nodes. As the layer starts to move, these phase discontinuities are smoothed out and shifted further downstream with the increase of Rm. As a result, the strongest phase variation is produced by the motion right downstream at the wave node, while the variation upstream remains relatively weak.

In the original concept, the flow rate is determined by measuring only the phase shift $\Delta_0\varphi$ between two observation points placed symmetrically with respect $x = 0$, which is the midpoint between two adjacent nodes of the mono-harmonic standing wave (3). The flow-induced phase shift vanishes at low velocities, which means $\delta_0\varphi \sim Rm$ for $Rm \ll 1$. It vanishes also at low ac frequencies, which means $\Delta_0\varphi \sim \bar{\omega}$ for $\bar{\omega} \ll 1$. This implies

$$\Delta_0\varphi \sim \bar{\omega} Rm \sim \sigma^2, \tag{4}$$

which means that at low velocities and low ac frequencies the phase shift varies quadratically with the electrical conductivity of the medium. The aim of this paper is to show how the variation of the flow-induced phase shift with the conductivity could be eliminated or at least significantly reduced. The idea is to achieve this by employing the additional information contained about the conductivity of medium in the phase shift between the sending coil and one of the receiving coils. We shall use the phase shift between the sending and the upstream receiving coil, which as noted above is less affected by the motion of the conducting medium than the downstream one, to scale the phase shift between the voltages in the receiving coils so that to reduce the effect of conductivity in the rescaled signal.

Let us start with $\bar{\omega} \ll 1$ discussed above. In this case, the reference phase shift between sending and receiving coils caused by the diffusion of the magnetic field through the conducting layer at rest is is expected to vary as $\varphi \sim \bar{\omega}$. It implies that the

conductivity can be eliminated from the phase shift (4) by the following rescaling

$$\Delta_2\varphi = \varphi_-^{-2}\Delta_0\varphi, \tag{5}$$

where $\Delta_0\varphi = \varphi_+ - \varphi_-$ is a difference between the phases measured at downstream and upstream observation points, which are denoted by φ_+ and φ_-, respectively. If we assume the ac frequency to be fixed, then the variation of the dimensionless frequency $\bar{\omega}$ means the variation of electrical conductivity, which, in turn, causes a variation of Rm at a fixed physical velocity. The quantity which for a fixed ac frequency varies with the physical velocity but not with the conductivity is the relative velocity $Rm/\bar{\omega} = v/(\omega H)$. It means that in the ideal case of a perfectly compensated conductivity effect, the rescaled phase shift $\delta_2\varphi$ is expected to depend only on $Rm/\bar{\omega}$ but not on $\bar{\omega}$.

As seen in figure 2, the rescaled phase shifts plotted versus the relative velocity $Rm/\bar{\omega}$ show only a weak dependence on the dimensionless frequency as long as $\bar{\omega}$ is sufficiently low. For low relative velocities, the variation of the rescaled phase shift with $\bar{\omega}$ remains rather weak up to $\bar{\omega} \sim 1$, which is consistent with the original assumption. The range of relative velocities which remains weakly affected by $\bar{\omega}$ depends on the location of the observation points. The closer the observation points to the wave nodes ($xk/\pi = \pm 0.5$), the shorter the range of the relative velocities for which $\delta_2\varphi$ remains insensitive to the increase of $\bar{\omega}$. In this range of relative velocities, the variation of the dimensionless frequency from 0.1 to 1, which is equivalent to the increase of the conductivity by an order of magnitude, results in a much smaller variation of the rescaled phase shift.

The results above show that rescaling (5) can compensate the effect of conductivity only at sufficiently low frequencies at which the variation of the reference phase is close to linear with $\bar{\omega}$. This scaling deteriorates at higher frequencies when the variation of the reference phase with $\bar{\omega}$ becomes non-linear due to the the shielding effect. In this case, the phase shift is $O(1)$ over the skin layer with the characteristic thickness $\sim \bar{\omega}^{-1/2}$. It means that the total phase shift due to the diffusion of magnetic field through the whole conducting layer with thickness $O(1)$ varies as $\varphi \sim \bar{\omega}^{1/2} \sim \sigma^{1/2}$. Since the external magnetic field in the form of a standing wave consists of two oppositely travelling waves, the motion of the layer is equivalent to the variation of the dimensionless frequency by $\sim Rm \ll 1$. The respective phase shift between two receiving coils can be estimated as

$$\Delta_0\varphi \sim \frac{\partial\varphi}{\partial\bar{\omega}} Rm \sim \bar{\omega}^{-1/2} Rm \sim \sigma^{1/2}.$$

It implies that for $\bar{\omega} \gtrsim 1$ the conductivity could be eliminated from the phase-shift between the receiving coils by rescaling it directly with the reference phase shift as

$$\Delta_1\varphi = \varphi_-^{-1}\Delta_0\varphi. \tag{6}$$

The rescaled phase shift $\Delta_1\varphi$ is plotted in figure 3 against the relative velocity for two different wavenumbers $k = 1$ and and $k = 0.5$ and various dimensionless frequencies. For $k = 1$, dependence of the rescaled phase shift on $\bar{\omega}$ is seen to diminish as the latter is increased above 1. For $k = 0.5$, which corresponds a wavelength of the applied magnetic

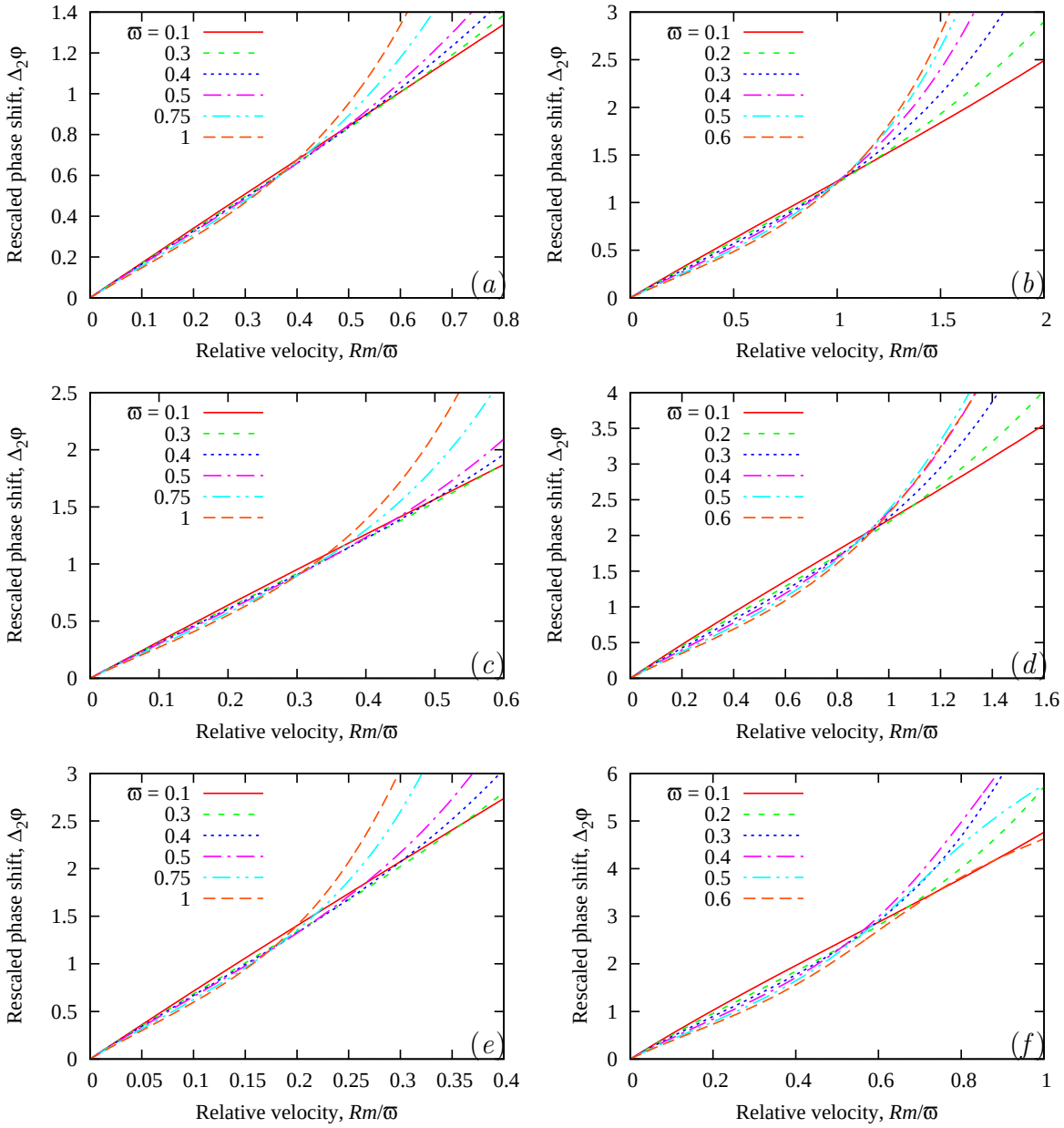

Figure 2. Rescaled phase shift $\Delta_2\varphi$ between two observation points placed below the layer at $\pm x = 0.2$ (a,b), 0.3 (c,d) and 0.4 (e,f) versus the relative velocity $Rm/\bar{\omega}$ for $k = 1$ (a,c,e) and $k = 0.5$ (b,d,f) at various dimensionless frequencies $\bar{\omega} \lesssim 1$.

field significantly larger than the thickness of the layer, the variation of $\Delta_1\varphi$ with $\bar{\omega}$ is practically insignificant starting from $\bar{\omega} = 1$.

3.2. External Magnetic Field Generated by a Pair of Straight Wires

In this section, we consider a more realistic external magnetic field which is generated by a couple of parallel wires with opposite currents separated by the horizontal distance $2s = 2$ and put at the height $h = 1$ above the layer, as shown in figure 1(b). For the

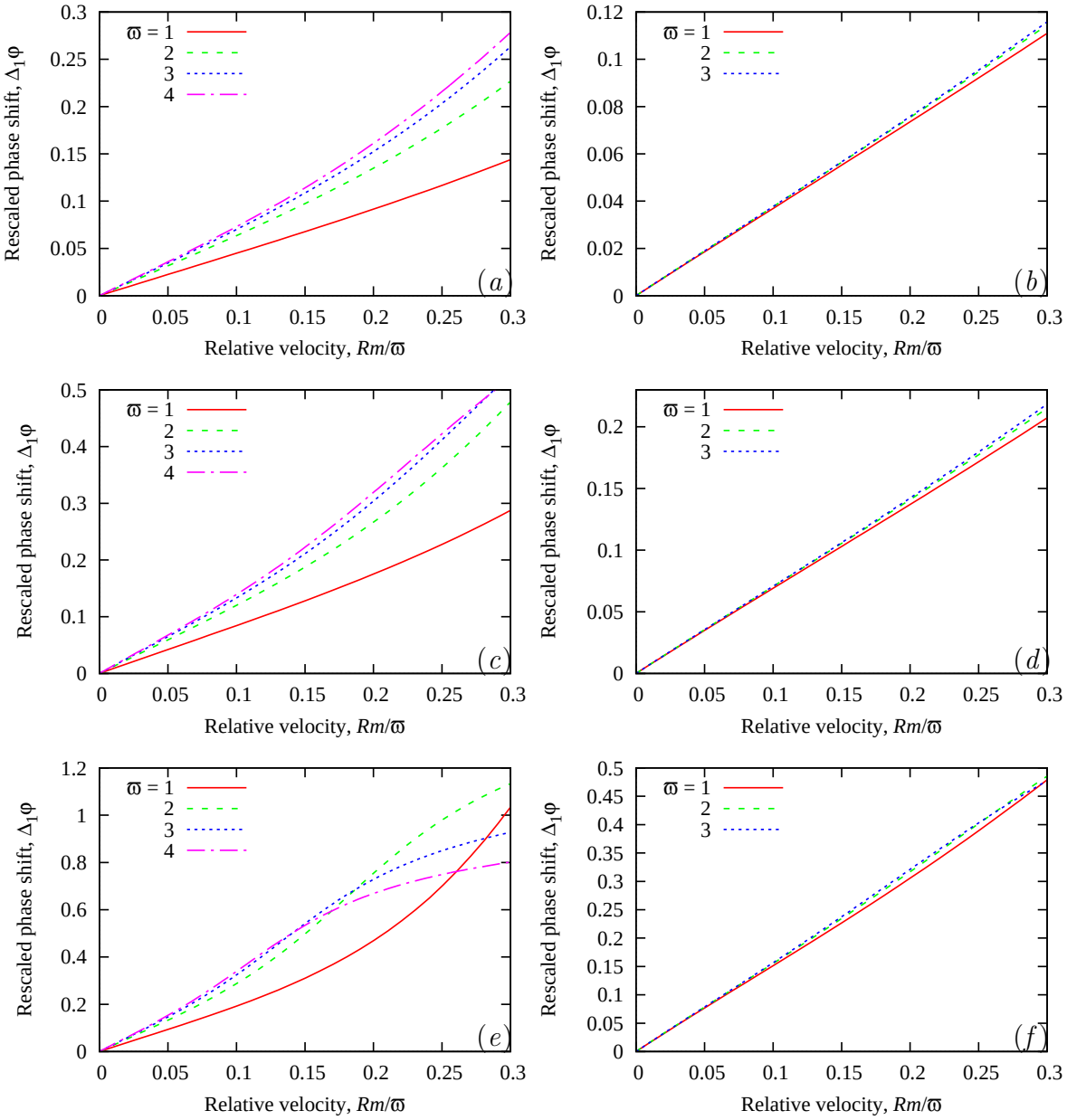

Figure 3. Rescaled phase shift $\Delta_1\varphi$ between two observation points placed below the layer at $\pm xk/\pi = 0.2$ (a,b), 0.3 (c,d) and 0.4 (e,f) versus the relative velocity $Rm/\bar{\omega}$ for $k = 1$ (a,c,e) and $k = 0.5$ (b,d,f) at various dimensionless frequencies $\bar{\omega} \gtrsim 1$.

layer at rest, the magnetic field distribution is mirror-symmetric with respect to the $x = 0$ plane, which, thus, is analogous to a node in the mono-harmonic standing wave considered in the previous section. Correspondingly, when the layer is at rest, there is a phase jump of π at $x = 0$. But in contrast to the previous case, the phase is no longer constant on both sides of the discontinuity and varies horizontally as well as vertically [13]. As a result, the range of dimensionless frequency where the phase sensitivity $K = \frac{1}{\pi}\frac{\partial\varphi}{\partial Rm}\big|_{Rm=0}$ [13], which is plotted in figure 4, varies more or less linearly with $\bar{\omega}$ and, thus, rescaling (5) could be applicable, is relatively short and limited to $\bar{\omega} \lesssim 0.02$.

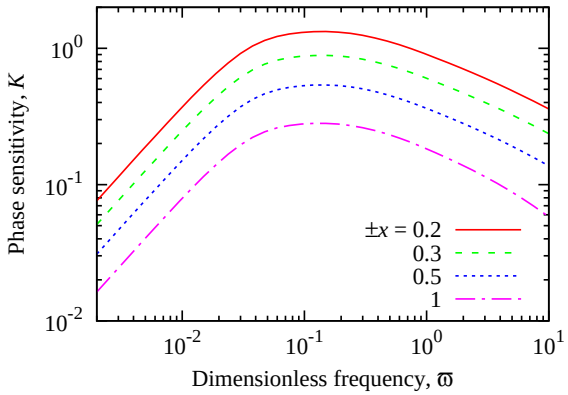

Figure 4. The phase sensitivity $K = \frac{1}{\pi}\frac{\partial\varphi}{\partial Rm}\Big|_{Rm=0}$ [13] versus the dimensionless frequency $\bar{\omega}$ at various observation points at the bottom of the layer .

Therefore, at $\bar{\omega} \sim 1$, which present the main interest from practical point of view, rescaling for the non-linear variation of the phase-shift (6) is expected to be applicable. This phase shift is plotted in figure 5 against the relative velocity for several locations of the observation points and various dimensionless frequencies. As seen, the rescaled phase shift $\Delta_1\varphi$ depends essentially on the relative velocity while its variation with $\bar{\omega}$ is relatively weak except for the largest separation of the observation points $x = \pm 2.5$ which is shown in figure 5(d). This deterioration of the rescaling at larger separations of observation points may be due to the horizontal variation of the reference phase mentioned above.

4. Summary and Conclusion

We have presented a concept of an improved phase-shift flowmeter which is much less susceptible to the variations of electrical conductivity of liquid metal than the original design of Priede et al. [13]. In the improved flowmeter we suggest to measure not only the internal phase shift between two receiving coils, but also the external phase shift between the sending coil and the upstream receiving coil. In contrast to the internal phase shift, which is induced by the flow, the external one depends mostly on the conductivity of the media but not so much on its velocity. We rescale the internal phase shift with the external phase shift to eliminate or at least strongly reduce the effect of conductivity on the operation of the flowmeter. Two different rescalings are found depending on the ac frequency. At low frequencies $\bar{\omega} \lesssim 1$, when the phase shift varies directly with the frequency, the conductivity can be eliminated by rescaling the internal phase shift with the square of the external phase shift. At higher ac frequencies $\bar{\omega} \gtrsim 1$, at which the shielding effect makes the variation of phase with the frequency non-linear, the conductivity can be eliminated by rescaling the internal phase shift directly with the external one. Note that for liquid sodium with $\sigma = 8.3 \times 10^6\,\mathrm{S/m}$ [10] and characteristic size $H \sim 0.1\,\mathrm{m}$, $\bar{\omega} \sim 1$ and $Rm \sim 1$ correspond to ac frequency $2\pi\omega \sim 60\,\mathrm{Hz}$ and

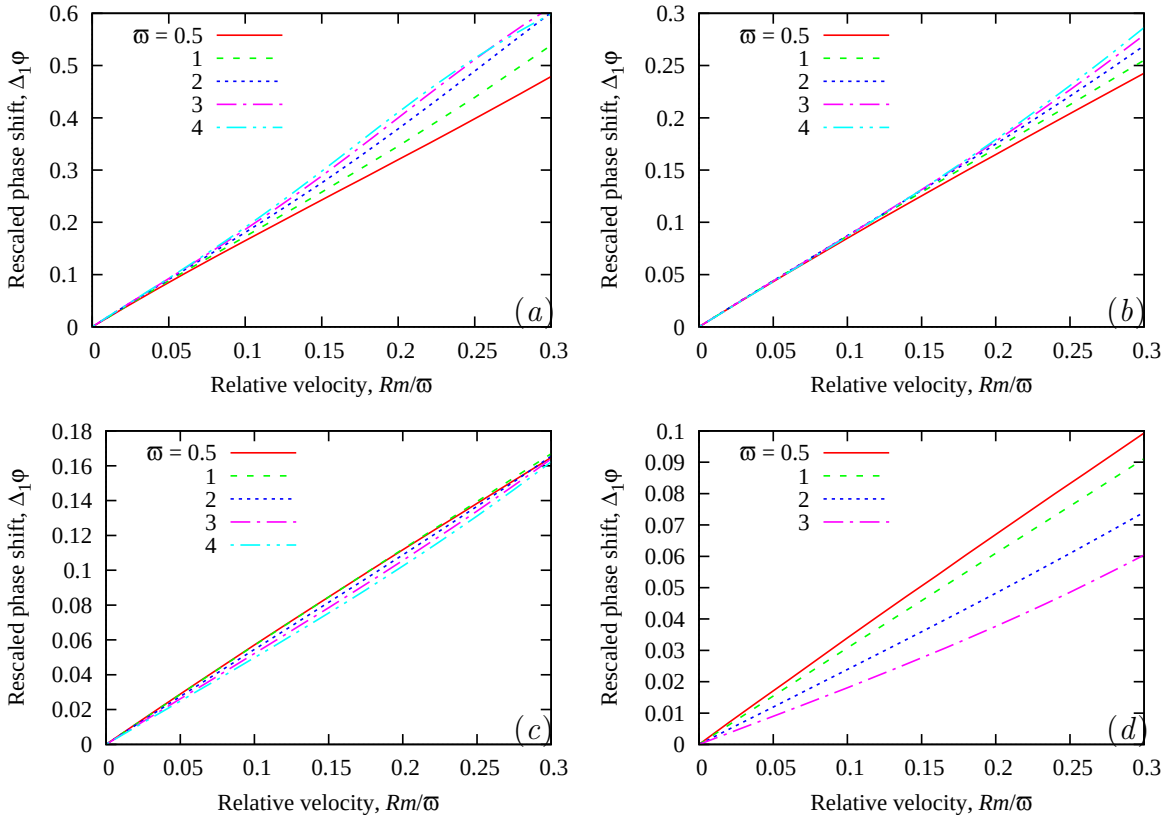

Figure 5. The rescaled phase shift $\Delta_1\varphi$ between two observation points placed below the layer at $\pm x = 0.5$ (a), 1 (b), 1.5 (c), and 2.5 (c) versus the relative velocity $Rm/\bar{\omega}$ at various dimensionless frequencies $\bar{\omega}$.

velocity $v \sim 1\,\mathrm{m/s}$, respectively.

The applicability of the first rescaling is limited to relatively low frequencies, especially for realistic sending coils which generate the magnetic field dominated by long-wave harmonics. A potential disadvantage of using low ac frequencies may be the relatively low sensitivity of the phase-shift flowmeter. From this point of view, it seems more attractive to operate the flowmeter in the frequency range with a moderate shielding effect where the second (direct) rescaling is applicable.

Our results may be useful for designing a next-generation phase-shift flowmeter with increased robustness to the variations of the electrical conductivity of liquid metal, which may be required in some metallurgical and other applications.

5. Appendix

5.1. Analytical solution for mono-harmonic external magnetic field

The amplitude distribution of the external magnetic (3) in free space, which follows from equation (1) with $\sigma = 0$, can be written as

$$\hat{A}_0(y;k) = C_0 e^{|k|(y-1)}, \tag{7}$$

where the constant

$$C_0 = \hat{A}_0(1;k) \tag{8}$$

defines the amplitude of the Fourier mode with the wavenumber k at the upper boundary of the layer. The external magnetic field (3) can be represented a superposition of two oppositely travelling waves

$$A_0(\boldsymbol{r},t) = \frac{1}{2}\left[A_0^+(\boldsymbol{r},t) + A_0^-(\boldsymbol{r},t)\right],$$

where $A_0^{\pm}(\boldsymbol{r},t) = \hat{A}_0(y)\cos(\omega t \pm kx)$, and the solution is written in a similar form as

$$A(\boldsymbol{r},t) = \frac{1}{2}\left[A^+(\boldsymbol{r},t) + A^-(\boldsymbol{r},t)\right],$$

where $A^{\pm}(\boldsymbol{r},t) = \Re\left[\hat{A}(y;\pm k)e^{ß(\omega t \pm kx)}\right]$. The solution in the free space above the layer ($y \geq 1$) is

$$\hat{A}(y;k) = \hat{A}_0(y;k) + \hat{A}_1(y;k), \tag{9}$$

where the first term represents the external field (7) and $\hat{A}_1(y;k) = C_1 e^{-|k|(y-1)}$ is the induced field. In the free space below the layer ($y \leq -1$), we have

$$\hat{A}(y;k) = C_3 e^{|k|(y+1)}. \tag{10}$$

In the conducting layer ($-1 \leq y \leq 1$), the solution takes the form

$$\hat{A}(y;k) = C_2\sinh(\kappa y) + D_2\cosh(\kappa y), \tag{11}$$

where $\kappa = \sqrt{k^2 + ß(\bar{\omega} + kRm)}$, $\bar{\omega} = \mu_0\sigma\omega H^2$ is a dimensionless ac frequency and $Rm = \mu_0\sigma v H$ is the magnetic Reynolds number, which represents a dimensionless velocity. The unknown constants, which are regarded as functions of the wavenumber k, are found from the boundary conditions (2) as follows

$$C_2 = C_0|k|/\left(|k|\sinh(\kappa) + \kappa\cosh(\kappa)\right) \tag{12}$$

$$D_2 = C_0|k|/\left(|k|\cosh(\kappa) + \kappa\sinh(\kappa)\right), \tag{13}$$

$$C_1 = D_2\cosh(\kappa) + C_2\sinh(\kappa) - C_0, \tag{14}$$

$$C_3 = D_2\cosh(\kappa) - C_2\sinh(\kappa). \tag{15}$$

5.2. Semi-analytical solution for external magnetic field generated by a pair of straight wires

Here we extended the solution above to the external magnetic field generated by a finite-size coil which consists of two parallel straight wires fed with an ac current of amplitude I_0 flowing in the opposite directions along the z-axis at distance $2s$ in the x-direction and placed at height h above the upper surface of the layer, as shown in figure 1(b). The free-space distribution of the vector potential amplitude having only the z-component, which is further scaled by $\mu_0 I_0$, is governed by

$$\boldsymbol{\nabla}^2 A_0 = -\delta(\boldsymbol{r} - h\boldsymbol{e}_y - s\boldsymbol{e}_x) + \delta(\boldsymbol{r} - h\boldsymbol{e}_y + s\boldsymbol{e}_x), \tag{16}$$

where $\delta(\boldsymbol{r})$ is the Dirac delta function and $\boldsymbol{r}$ is the radius vector. The problem is solved by the Fourier transform $\hat{A}(y;k) = \int_{-\infty}^{\infty} A(x,y)e^{ßkx}$ ẋ, which yields

$$\hat{A}_0(y;k) = ße^{-|k(y-h)|}\sin(ks)/|k|. \tag{17}$$

The solution for a Fourier mode with the wave number k for the regions above, below and inside the layer is given, respectively, by expressions (9, 10) and (11) with the coefficients (12)–(15) containing the constant C_0, which is defined by substituting (17) into (8). Then the spatial distribution of the complex vector potential amplitude is given by the sum of Fourier modes, which is defined by the inverse Fourier transform $A(x,y) = \frac{1}{2\pi}\int_{-\infty}^{\infty}\hat{A}(y;k)e^{-ßkx}$ k̇ and can efficiently be calculated using the Fast Fourier Transform.

References

[1] Baker, R. [2016]. *Flow Measurement Handbook*, Cambridge University Press.

[2] Bucenieks, I. [2005]. Modelling of rotary inductive electromagnetic flowmeter for liquid metals flow control, *Proc. 8th Int. Symp. on Magnetic Suspension Technology, Dresden, Germany, 26–28 September*, pp. 204–8.

[3] Cowley, M. [1965]. Flowmetering by a motion-induced magnetic field, *J. Sci. Instrum.* **42**(6): 406.

[4] Faraday, M. [1832]. Experimental researches in electricity, *Phil. Trans. R. Soc. Lond.* **122**: 125–162.

[5] Feng, C., Deeds, W. and Dodd, C. [1975]. Analysis of eddy-current flowmeters, *J Appl Phys* **46**(7): 2935–2940.

[6] Forbriger, J. and Stefani, F. [2015]. Transient eddy current flow metering, *Meas. Sci. Technol.* **26**(10): 105303.

[7] Hussain, Y. and Baker, R. [1985]. Optimised noncontact electromagnetic flowmeter, *J. Phys. E: Sci. Instrum.* **18**(3): 210.

[8] Lehde, H. and Lang, W. [1948]. Device for measuring rate of fluid flow, US Patent 2,435,043.

[9] McHale, E. J., Hussain, Y., Sanderson, M. and Hemp, J. [1985]. Capacitively-coupled magnetic flowmeter, US Patent 4,513,624.

[10] Müller, U. and Bühler, L. [2001]. *Magnetofluiddynamics in Channels and Containers*, Springer.

[11] Poornapushpakala, S., Gomathy, C., Sylvia, J., Krishnakumar, B. and Kalyanasundaram, P. [2010]. An analysis on eddy current flowmeter–a review, *Recent Advances in Space Technology Services and Climate Change (RSTSCC), 2010*, IEEE, pp. 185–188.

[12] Priede, J., Buchenau, D. and Gerbeth, G. [2009]. Force-free and contactless sensor for electromagnetic flowrate measurements, *Magnetohydrodynamics* **45**(3): 451–458.

[13] Priede, J., Buchenau, D. and Gerbeth, G. [2011a]. Contactless electromagnetic phase-shift flowmeter for liquid metals, *Meas. Sci. Technol.* **22**(5): 055402.

[14] Priede, J., Buchenau, D. and Gerbeth, G. [2011b]. Single-magnet rotary flowmeter for liquid metals, *J. Appl. Phys.* **110**(3): 034512.

[15] Schulenberg, T. and Stieglitz, R. [2010]. Flow measurement techniques in heavy liquid metals, *Nucl. Eng. Des.* **240**(9): 2077–2087.

[16] Shercliff, J. [1960]. Improvements in or relating to electromagnetic flowmeters, GB Patent 831226.

[17] Shercliff, J. [1987]. *The Theory of Electromagnetic Flow-Measurement*, Cambridge Science Classics, Cambridge University Press.

[18] Spencer, M. and Denison, A. [1959]. The square-wave electromagnetic flowmeter: theory of operation and design of magnetic probes for clinical and experimental applications, *IRE Trans. Med. Electron.* **ME-6**(4): 220–228.

[19] Stefani, F. and Gerbeth, G. [2000]. A contactless method for velocity reconstruction in electrically conducting fluids, *Meas. Sci. Technol.* **11**(6): 758.

[20] Stefani, F., Gundrum, T. and Gerbeth, G. [2004]. Contactless inductive flow tomography, *Phys. Rev. E* **70**(5): 056306.

[21] Thess, A., Votyakov, E., Knaepen, B. and Zikanov, O. [2007]. Theory of the lorentz force flowmeter, *New J. Phys.* **9**(8): 299.

[22] Velt, I. and Mikhailova, Y. V. [2013]. Magnetic flowmeter of molten metals, *Meas. Tech.* **56**(3): 283.